

On-chip silicon-based active photonic molecules by complete photonic bandgap light confinement

Bo Qian,^{1,2,3,a)} Kunji Chen,¹ San Chen,¹ Wei Li,¹ Xiangao Zhang,¹ Jun Xu,¹ Xinfan Huang,¹ Lorenzo Pavesi,² and Chunping Jiang³

¹State Laboratory of Solid State Microstructures and Department of Physics, Nanjing University, Nanjing 210093, People's Republic of China

²Laboratorio di Nanoscienze, Dipartimento di Fisica, Università di Trento, Via Sommarive 14, I-38050, Povo (Trento), Italy

³Suzhou Institute of Nano-tech and Nano-bionics (SINANO), Chinese Academy of Sciences, Suzhou 215125, People's Republic of China

(Received 28 February 2011; accepted 28 June 2011; published online 22 July 2011)

We demonstrate an on-chip silicon-based active photonic molecule (PM) structures formed by two coupled photonic quantum dots with complete photonic bandgap (PBG) light confinement. The photonic quantum dots are grown by conformal deposition of amorphous silicon nitride multilayers on patterned substrates. A fine structure of the coupled optical modes in PMs has been observed which shows similarity to the electronic bonding (BN) and antibonding (ABN) states in a molecule. © 2011 American Institute of Physics. [doi:10.1063/1.3614548]

Photonic molecule (PM)^{1,2} mimics the electronic states in chemical molecules by using resonant modes in coupled microcavities. This concept is another strategy to manipulate the density of states of photons in a material which differs from photonic crystals or photonic bandgap (PBG) materials.^{3,4} In PBG materials, the periodic modulation of the refractive index can be treated as a weak additional potential which governs the propagation of light waves. On the other hand, confining light in a small volume, e.g., in a microcavity of wavelength dimension represents a strong perturbation to the photon mode density which is similar to what happens for electrons confined in quantum dots. For this reason, these systems are called photonic quantum dots.^{5,6} A natural evolution of the concept is to consider coupled photonic quantum dots, i.e., photonic molecules.^{1,2,7} There are many potential applications for PMs, e.g., low-threshold lasers,⁸ optical switches,⁹ quantum information science,¹⁰ and phonon laser.¹¹

However, compared to PBG materials, research on PMs is quite limited due to their fabrication complexity. The use of coupled microspheres is complicated by the difficulty of on-chip integration.^{1,12,13} Microdisks require a precise control of the coupling distance between disks^{8–10} and have a complex mode density with high order modes which complicates the picture, where the analogy to simple chemical molecules is lost. Microcavities in PBG materials have a plain photon mode density and allow an easy control of the coupling. The coupling can be easily controlled because the optical mode is confined by Bragg reflections, which have a greater penetration depth in the confining material than the one due to total internal reflection as it occurs in microdisks.¹⁴ But coupled microcavities in 3D photonic crystals or complete PBG materials are still a big challenge in state of the art photonic crystal technologies.^{15–18} In this paper, we

propose to use conformal deposition method to form on-chip silicon-based 3D PMs with complete PBG light confinement.

The PM samples are prepared by two basic steps. The first is to etch mesas on silicon substrates.⁶ The second is to produce PMs by growing coupled microcavities on the initial etched substrates by using conformal deposition of amorphous silicon nitride films (*a*-SiN). The mesas are designed to square shapes with lateral size of 1 μm , 2 μm , 3 μm , and 4 μm and a height of 400 nm. A sequence of *a*-SiN films is then conformably grew on these mesas by plasma enhanced chemical vapor deposition (PECVD). Ammonia (NH₃) and silane (SiH₄) gas mixtures were used as the reaction sources, and the gas ratio $R = (\text{NH}_3/\text{SiH}_4)$ was changed to control the film compositions.

Following is the growing process of the coupled microcavities: A periodic sequence of 5 periods of quarter wavelength thick *a*-SiN films with low refractive index ($n = 1.9$) and high index ($n = 2.8$) was deposited by alternatively using a gas ratio $R = 8$ and $R = 0.5$. This sequence forms a distributed Bragg reflector (DBR). Due to their amorphous nature, the films grew following the morphology of the mesa. Then, an active *a*-SiN luminescent layer with index ($n = 2.1$) was deposited by using gas ratio $R = 2$. This layer shows a room-temperature broad luminescence emission with a peak wavelength of 720 nm and a bandwidth of 100 nm. For this reason, the central wavelength of the microcavity is designed to be $\lambda = 750$ nm. The active layer was separated by 2.5 periods DBR from the second $\lambda/2$ active layer. Finally, a 5 periods DBRs finished the growth. The details of each layer can be found in Table I.

3D finite-difference time-domain (FDTD) simulations of the PM on 1 μm side mesa were performed by using the CRYSTALWAVE software of Photon Design.

Figure 1(a) shows the scanning electron micrograph (SEM) of a PM sample, which is conformably deposited on a square mesa of width of $W = 1$ μm . A bump is observed in correspondence of the mesa. The surface appears to be smooth. The original square form of the pattern is changed

^{a)}Author to whom correspondence should be addressed. Electronic mail: bqian2010@sinano.ac.cn. Tel.: +86 512 62872727. FAX: +86 512 62603079.

TABLE I. Layer sequence and optical parameters.

Periods	Layer	NH ₃ /SiH ₄ flux ratio	Refractive index	Thickness (nm)	Optical gap (eV)
5	$\lambda/4$ a-SiN _x	8	1.9	99	3.8
	$\lambda/4$ a-SiN _y	0.5	2.8	67	2.0
1	$\lambda/2$ a-SiN _z	2	2.1	179	2.5
2.5	$\lambda/4$ a-SiN _x	8	1.9	99	3.8
	$\lambda/4$ a-SiN _y	0.5	2.8	67	2.0
1	$\lambda/2$ a-SiN _z	2	2.1	179	2.5
5	$\lambda/4$ a-SiN _x	8	1.9	99	3.8
	$\lambda/4$ a-SiN _y	0.5	2.8	67	2.0

in a dome like shape due to film bending at the edge of the mesa. The dome diameter is $2 \mu\text{m}$, while the height is 400 nm which inherits from the mesa. In Fig. 1(b), the layer sequence is observed by a cross-section transmission electron microscopy (TEM) image. The TEM image is compared to the schematic picture of Fig. 1(c). It can be clearly observed that the films have grown conformably on the mesa by preserving the layer sequence. An evolution of the radius of curvature of the deposited film at the mesa edges is observed: the first layers have small curvature radii while the last layers have large curvature radii. This is the main difference with respect to Fig. 1(c). The two active layers, which form the PM, can be clearly observed in Fig. 1(b). It is worth to note that photons in these layers are confined both vertically as well as laterally by the DBR layers, since these last bends at the edge of the mesa. In this way, a 3D photon confinement in the active layer is achieved. Note that the lateral extension of the active layer is defined by the side DBRs. Thus, the top active layer is larger than the bottom one; the size difference depends on the distance between them. In the following, we name the PM by using the average size of the active layers, i.e., the mesa side $+0.5 \mu\text{m}$. 3D FDTD simulation was performed for $1.5 \mu\text{m}$ PM. Each layer is described by using the parameters listed in Table I. The initial condition is a Gaussian pulse centered at 750 nm with a transverse polarization (electric field vector E_z) excited from the bottom of the PM structure. Fig. 1(d) shows top-view images of the amplitudes of the computed optical field distribution in the two active layers of the PM structure for the bonding (bottom) and antibonding (up) states, when a complete PBG confinement is assumed. It is observed that in the top and bottom active layers, the field exhibit σ^* and σ orbital like distributions, respectively. Note that since the real active layers of PMs are curved at the edge of the

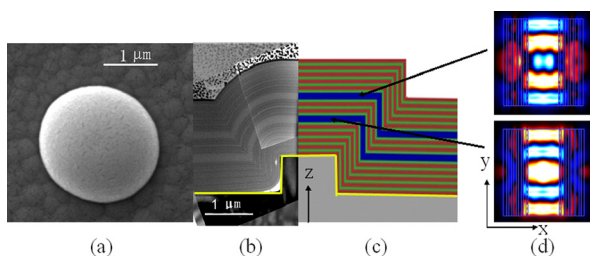


FIG. 1. (Color online) (a) Scanning electron micrograph of the top-view of PM on chip; (b) cross-section transmission electron microscopy image of PM; (c) schematic illustration of the PM. Along the Z-axis, there are substrate with square mesa and the SiN layer sequences which described in Table I. The white line cross (b) and (c) is drawn to highlight the pre-etched substrate; and (d) the in-plane field distribution in top and bottom active layers of PM $1 \mu\text{m}$.

mesas, the confinement effect by the side DBRs should be weaker than the simulation model; thus the real field distribution in active layers will expand to a larger space than the simulation result.

Room temperature micro-photoluminescence ($\mu\text{-PL}$) measurements were performed with the 488 nm line of an Ar laser. The results are presented in Figure 2. It is observed that the emission of the PM is characterized by two main bands with undulating high energy shoulders. The two bands are due to the resonant splitting of the two cavity modes due to the coupled cavities. This coupling is caused by the presence of the 2.5 period central DBR. Hence, in analogy to the chemical molecule, the peaks in the two emission bands can be noted as bonding (BN) modes for the low energy band and antibonding (ABN) modes for the high energy band. The energy positions of the BN and ABN modes decrease, while their separation increases as the lateral size of the PM decreases. In addition, the small undulations observed on the high energy shoulders of the BN and ABN emissions due to mode splitting become more resolved and spaced when the PM lateral size decreases from $4.5 \mu\text{m}$ to $1.5 \mu\text{m}$. This is due to a more effective in-plane confinement by the side DBR. It is also observed that the mode splitting is deeper and clearer in the BN emission than in the ABN emission band. This should come from the asymmetric mode coupling by the different sized active layers. The sharpest peak appears in the spectra of the $2.5 \mu\text{m}$ PM, with a linewidth of 5 meV (2 nm) and a quality factor ($Q = \Delta\lambda/\lambda$) of 350. This Q is more than 6 times larger than what we found in one-dimensional

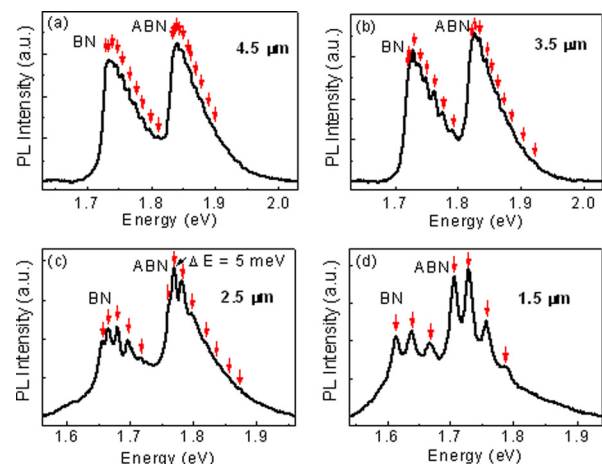


FIG. 2. (Color online) Room temperature PL spectra from PMs with different lateral size. The lateral size of active layers was estimated $0.5 \mu\text{m}$ larger than that of the substrate. The arrows are marked above the peak positions for eye guiding.

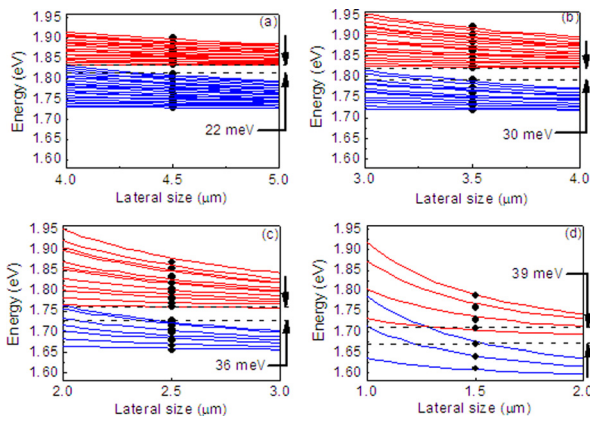


FIG. 3. (Color online) (a-d) Comparison of the experimental data (solid dots) and calculated data (solid lines) for the fine energy levels of PMs. The energy band gaps are marked by dotted lines, which dividing the BN (lower) and ABN (up) bands.

microcavities.⁶ Contrary to expectation, the quality factor decreases in the 1.5 μm PM probably due to the relevance of side wall roughness for this PM size.

Based on this analogy, a simple modeling has been derived. Let us consider a 3D confinement in a single photonic molecule. The energy of the different modes is^{5,6}

$$E_{ph} = \frac{\hbar c}{n} \sqrt{k_{1,2}^2 + k_x^2 + k_y^2},$$

where $k_{1,2} = 2\pi n/\lambda_{1,2}$ denote the vertical wavevectors of the bonding and antibonding modes in the two active layers, while k_x and k_y are the in-plane wavevectors. The in-plane wavevectors are quantized by the lateral confinement

$$k_{x,y} = (m_{x,y} + 1) \frac{\pi}{L},$$

where $m_{x,y} = 0, 1, 2, 3, \dots$ corresponds to the lateral quantum numbers and L is the lateral width of the square shaped structures. Note that it is assumed that L is the same for the two active layers.

A comparison between the model and the experiments is reported in Fig. 3. The fitting parameters $\lambda_{1,2}$ are listed in Table II, n uses the refractive index of the active layer (2.1). The fine modes in the BN and ABN bands are represented by curves. Experimental data are shown as dots. A good correspondence is observed between modeling and experiments. Moreover, it is observed that for the lowest energy modes in both bands, the agreement between experiment and theory is rather good, while for the higher energy modes a small deviation exists. The band gap of PM can be defined as the distance between the highest energy mode for the lower band and the lowest energy mode of the higher band, analogously to the definition of the HOMO-LUMO gap in chemistry. There is a clear increase of the band gap of PMs (Fig. 4) as well as a clear decrease of the gap center position (Fig. 4) when the lateral size of the PM decreases. Such a trend is a

TABLE II. The fitting parameters for the fine modes of PMs.

PMs	4.5 μm	3.5 μm	2.5 μm	1.5 μm
λ_1	677 nm	682 nm	708 nm	738 nm
λ_2	718 nm	723 nm	752 nm	784 nm

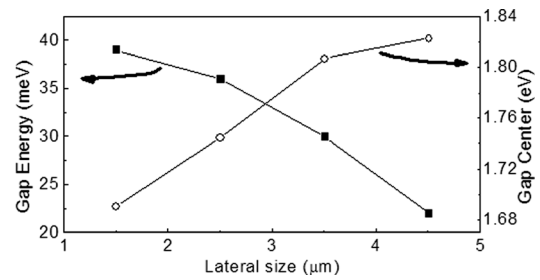


FIG. 4. The PM band gap energy (Solid square) and gap center position (empty circle) evolution versus the PM lateral size. The lines are drawn for eye guiding.

consequence of the increased photon modes as well as the binding energy of the photonic molecules.

3D PBG PMs have been obtained by conformal deposition method. By changing the size of the mesa, a rich phenomenology of the molecule-like fine energy modes has been observed. A simple model has been proposed to analyze the data, where it is observed that the larger is the photon confinement, the wider is the mode splitting. In the future, it will be interesting to investigate whether the PM can be used for lasing in silicon-based materials.¹⁹ A possibility could be to elaborate on the concept used in the two-level phonon laser system, where the traditional roles of the material (laser medium) and cavity modes (lasing field) are reversed: the medium is purely optical, while the laser field is provided by the materials as a phonon mode.¹¹

The author would like to thank Professor Ting-Chang Chang, National Sun Yat-Sen University, for preparing TEM photograph and also acknowledges the financial support of NSFC (Nos. 60806015, 10974091) and “973” project (Nos. 2007CB613401, 2010CB934100).

- ¹E. Lidorikis, M. M. Sigalas, E. N. Economou, and C. M. Soukoulis, *Phys. Rev. Lett.* **81**, 1405 (1998).
- ²M. Bayer, T. Gutbrod, J. P. Reithmaier, A. Forchel, T. L. Reinecke, P. A. Knipp, A. A. Dremin, and V. D. Kulakovskii, *Phys. Rev. Lett.* **81**, 2582 (1998).
- ³S. John, *Phys. Rev. Lett.* **58**, 2486 (1987).
- ⁴E. Yablonovitch, *Phys. Rev. Lett.* **58**, 2059 (1987).
- ⁵J. P. Reithmaier, M. Rohner, H. Zull, F. Schafer, A. Forchel, P. A. Knipp, and T. L. Reinecke, *Phys. Rev. Lett.* **78**, 378 (1997).
- ⁶S. Chen, B. Qian, K. Chen, X. Zhang, J. Xu, Z. Ma, W. Li, and X. Huang, *Appl. Phys. Lett.* **90**, 174101 (2007).
- ⁷T. Mukaiyama, K. Takeda, H. Miyazaki, Y. Jimba, and M. Kuwata-Gonokami, *Phys. Rev. Lett.* **82**, 4623 (1999).
- ⁸A. Nakagawa, S. Ishii, and T. Baba, *Appl. Phys. Lett.* **86**, 041112 (2005).
- ⁹S. Ishii and T. Baba, *Appl. Phys. Lett.* **87**, 181102 (2005).
- ¹⁰I. S. Grudin, H. Lee, O. Painter, and K. J. Vahala, *Phys. Rev. Lett.* **104**, 083901 (2010).
- ¹¹H. J. Kimble, *Nature* **453**, 1023 (2008).
- ¹²M. D. Barnes, S. M. Mahurin, A. Mehta, B. G. Sumpter, and D. W. Noid, *Phys. Rev. Lett.* **88**, 015508 (2001).
- ¹³Y. P. Rakovich, J. F. Donegan, M. Gerlach, A. L. Bradley, T. M. Connolly, J. J. Boland, N. Gaponik, and A. Rogach, *Phys. Rev. A* **70**, 051801 (2004).
- ¹⁴S. Ishii, K. Nozaki, and T. Baba, *Jpn. J. Appl. Phys.* **45**, 6108 (2006).
- ¹⁵P. V. Braun, S. A. Rinne, and F. Garcia-Santamaria, *Adv. Mater.* **18**, 2665 (2006).
- ¹⁶M. Qi, E. Lidorikis, P. T. Rakich, S. G. Johnson, J. D. Joannopoulos, E. P. Ippen, and H. I. Smith, *Nature* **429**, 538 (2004).
- ¹⁷S. A. Rinne, F. Garcia-Santamaria, and P. V. Braun, *Nature Photon.* **2**, 52 (2008).
- ¹⁸K. Aoki, D. Guimard, M. Nishioka, M. Nomura, S. Iwamoto, and Y. Arakawa, *Nature Photon.* **2**, 688 (2008).
- ¹⁹L. Pavesi, L. Dal Negro, C. Mazzoleni, G. Franzo, and F. Priolo, *Nature* **408**, 440 (2000).